Imidazolylidene Cu(II) complexes: synthesis using imidazolium carboxylate precursors and structure rearrangement pathways

Nathalie Ségaud,[a] Jonathan McMaster,[b] Gerard van Koten,[c] Martin Albrecht*,[a]

a) Department of Chemistry & Biochemistry, University of Bern, Freiestrasse 3, 3012 Bern, Switzerland
b) School of Chemistry, University of Nottingham, University Park, Nottingham, NG7 2RD, UK
c) Organic Chemistry and Catalysis, Debye Institute for Materials Science, Faculty of Science, Utrecht University, 3584CG Utrecht, The Netherlands

Key words: copper(II); imidazolylidene; carbene hyperfine coupling; decarboxylation; coordinative lability; ligand redistribution

Abstract

Copper(II) complexes of type (NHC)CuX_2 (X = OAc, Cl, Br, BF_4, NO_3) bearing monodentate N-heterocyclic carbenes (NHCs) were prepared by *in situ* decarboxylation of imidazolium carboxylates as a new synthetic methodology for Cu(II)-NHC complexes. In contrast to the classical deprotonation method, the decarboxylation protocol does not require anaerobic conditions and provides access to complexes with NHCs that are unstable as free carbenes such as *N,N'*-diisopropyl-imidazolylidene and *N,N'*-dimethyl-imidazolylidene. Spectroscopic evidence of the formation of the $Cu–C_{NHC}$ bond is provided by UV-vis and EPR, in particular by the 44 MHz carbene hyperfine coupling constant using a ^{13}C-labelled imidazolylidene ligand. A variation of the nature of the carbene N-substituents and the anions bound to the Cu(II) center is possible with this methodology. These variations strongly influence the stability of the complexes. Structural rearrangement and ligand reorganization was observed during re-crystallisation, which are comprised of heterolytic $Cu–C_{NHC}$ bond dissociation for unstable NHC ligands as well as homolytic Cu–X bond cleavage and disproportionation reactions depending on the nature of the anion X in the copper complex.

Introduction

N-Heterocyclic carbenes (NHCs)[1] have emerged as ligands for transition metals to perform a multitude of catalytic transformations.[2] In particular, Cu-containing NHC complexes have been used as catalysts for a broad range of reactions such as the Huisgen cycloaddition, hydrosilylation, carboxylation, olefination, C–C bond cleavage, C–C and C–N coupling reactions, in which the active species is Cu(I).[3] While soft-acid soft-base Cu(I)–C interactions lead to highly stable Cu(I)-NHC complexes, less favourable intermediate/hard-soft Cu(II)–C interactions make the isolation of Cu(II)-NHC complexes difficult. Consequently and in contrast to low valent copper(I) NHC complexes, which are widely known,[3–5] higher valent Cu(II)-NHC analogues are very rare. Most of the few examples reported so far employ tethered-NHC ligands to favour coordination to the Cu(II) center (for example complexes **A–D**,[6–9] Fig. 1). These Cu(II)-NHC complexes are typically prepared by transmetalation using an NHC transfer reagent or by direct complexation to the isolated free carbene.[6–16] Complexation of Cu(II) by unsupported monodentate NHC ligands has been explored little with only (**1**)$Cu(OAc)_2$ being authenticated by X-ray crystallography (**E**, Fig. 1).[12]

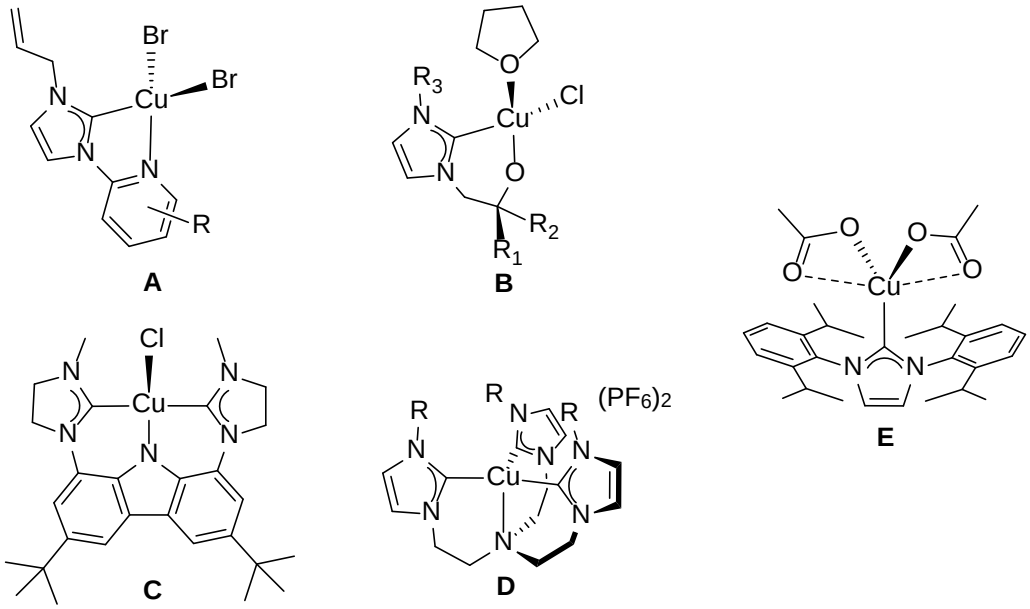

Figure 1. Selected examples of reported Cu(II)-NHC complexes bearing tethered-NHC ligands (**A–D**) or monodentate NHC ligand (**E**).

The use of carboxylate precursors of NHCs has been demonstrated for the preparation of NHC metal complexes of Ir, Rh, Ru, Pd, Pt, and Cu, and showed a high tolerance to water.[17–20] An advantage of this method is the generation of the desired complex through an *in situ*

decarboxylation process induced by the metal precursor, which avoids the handling of the free carbene. Inspired by the early work of Saegusa and Cahiez who demonstrated that Cu(II) is promoting decarboxylative Cu–C bond formation with, e.g., benzoate,[21,22] we envisaged the preparation of a variety of Cu(II)-NHC complexes using different imidazolium carboxylate precursors and diverse Cu(II) salts. Herein we describe a series of compounds using this approach and their characteristic EPR and UV/vis spectroscopic properties in solution. In particular, we demonstrate that their preparation and stability is distinctly influenced by the nature of the N-wingtip groups of the NHC ligands and by the anion of the copper precursor.

Results and Discussion

New synthetic route using an imidazolium carboxylate as NHC precursor. We have applied the decarboxylation strategy for the synthesis of the known Cu(II)-NHC complex (**1**)Cu(OAc)$_2$[12] (Scheme 1). When starting from the carboxylate precursor **1-CO$_2$**, the desired complex (**1**)Cu(OAc)$_2$ was obtained in similar yields as via the deprotonation route (63%), yet in only one single step and in an aerobic atmosphere.[23] This is in contrast to the published route that requires the deprotonation of the imidazolium salt **1H.Cl** and isolation of the air-sensitive free carbene **1**, followed by its reaction with Cu(OAc)$_2$ under inert and dry conditions.[12]

Scheme 1. Synthesis of complex (**1**)Cu(OAc)$_2$ following either the deprotonation (top) or the decarboxylation (bottom) routes starting from ligands **1H.Cl** and **1-CO$_2$**, respectively.

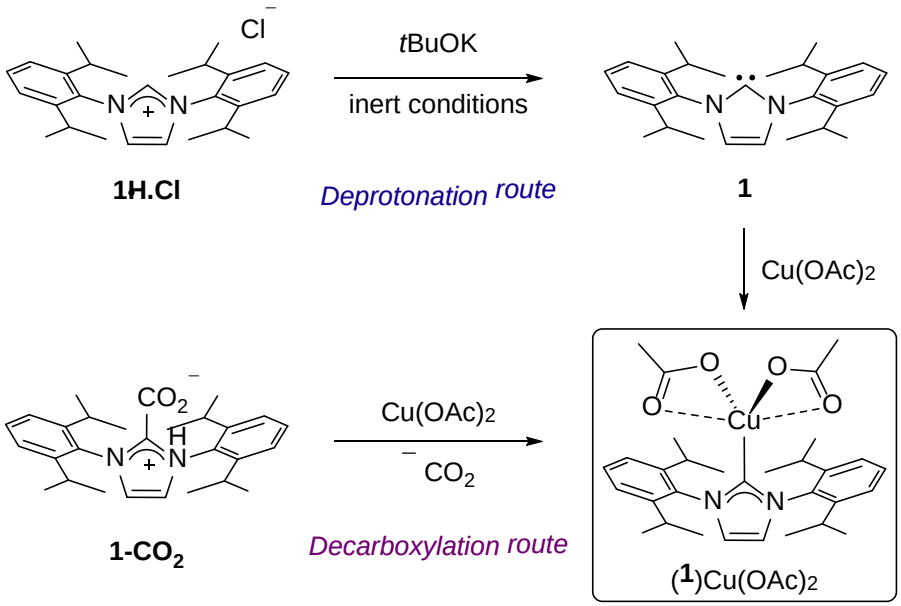

Support for the formation of (**1**)Cu(OAc)$_2$ was obtained by infrared spectroscopic analysis (Fig. 2, see Figure S2 for full spectra). The vibration bands at 1674 and 1305 cm^{-1} (assigned to the carboxylate functional group for the ligand precursor **1-CO$_2$**) are absent in the spectrum of (**1**)Cu(OAc)$_2$, suggesting that the CO$_2$ functional group is no longer pendant to the ligand framework. Moreover, the acetate bands in the 1600 cm^{-1} area are sharper and more clearly defined than the broad features in the precursor Cu(OAc)$_2$ salt, indicative of a better defined ligand arrangement in the complex due to NHC coordination to the Cu(II) center. The identity of complex (**1**)Cu(OAc)$_2$ prepared via the decarboxylation route was verified by comparison with an authentic sample of (**1**)Cu(OAc)$_2$ prepared by the deprotonation route as reported in the literature.[12] Both samples were recrystallized from a saturated CH_2Cl_2 solution by pentane diffusion and the crystals were analyzed by powder X-ray diffraction. The powder X-ray diffractograms of both samples of (**1**)Cu(OAc)$_2$ showed well resolved crystalline intensities, in a monoclinic crystal pattern with C2/c space group (Figure 3). The identical intensities in the 8–30° 2θ range for both samples indicate that the structure of both crystalline species is the same. The diffractogram features a prominent maximum at 2θ = 8.835° with corresponding *d* spacing value of 10.001 Å, and strong intensities at 11.090 and 11.277°. Significantly, the diffractogram of (**1**)Cu(OAc)$_2$ calculated from the reported single crystal X-ray diffraction data[12] shows an essentially identical pattern especially in the low theta range with strong intensities at 8.843, 11.077 and 11.272° (Figure 3; Tables S1, S2).

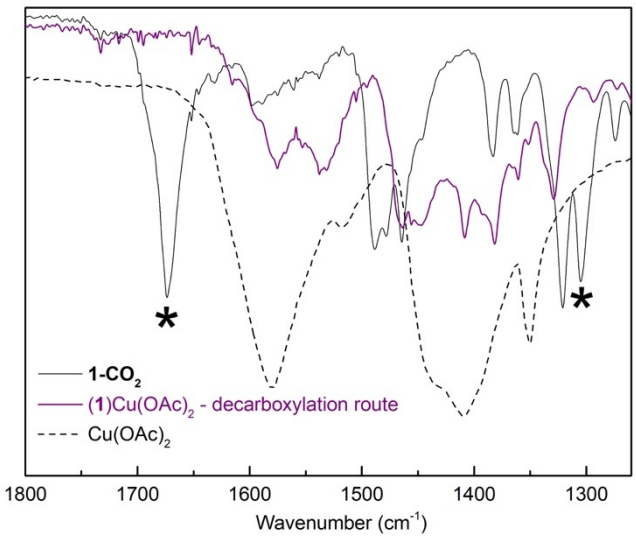

Figure 2. ATR-FTIR spectrum in the 1250–1800 cm^{-1} range of solid (**1**)Cu(OAc)$_2$ synthesized following the decarboxylation route (purple), compared to spectra of **1-CO$_2$** (black, solid) and Cu(OAc)$_2$ (black, dotted). The asterisks denote the diagnostic vibration bands related to the carboxylate group in the imidazolium carboxylate at 1674 and 1305 cm^{-1}.

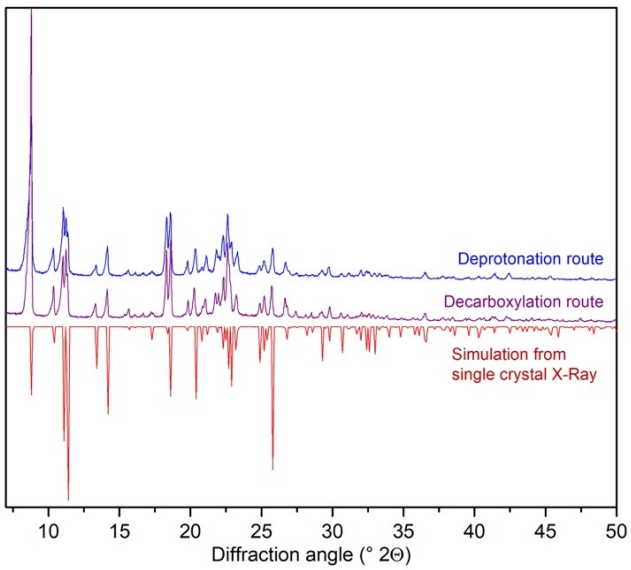

Figure 3. Powder X-Ray diffractograms of complexes (**1**)$Cu(OAc)_2$ synthesized following the deprotonation (blue) or decarboxylation (purple) route, compared to the calculated diffractogram (red) from the reported structure (CCDC No 274568).

Exploiting the decarboxylation route for variation of the NHC ligand. The new synthetic route was applied to the synthesis of (NHC)$Cu(OAc)_2$ complexes using NHCs with different N-wingtip groups, which vary from bulky mesityl (Mes) (**2**) to smaller and stronger electron-donating alkyl groups such as *i*Pr (**3**) and Me (**4**) (Scheme 2). The corresponding carboxylate precursors **2-CO$_2$**, **3-CO$_2$**, and **4-CO$_2$**, respectively, were synthesized following reported procedures.[17,24] Exposure to $Cu(OAc)_2$, afforded complexes (**2**)$Cu(OAc)_2$, (**3**)$Cu(OAc)_2$ and (**4**)$Cu(OAc)_2$, which were isolated as deep blue powders by Et_2O precipitation in moderate to good yields (50–93%). The solids are hygroscopic as observed by elemental analysis, in particular complexes (**3**)$Cu(OAc)_2$ and (**4**)$Cu(OAc)_2$ that contain aliphatic substituents on the NHC ligand. Therefore, these complexes were stored under inert atmosphere for preparing analytical samples.

Attempts to prepare these (NHC)$Cu(OAc)_2$ complexes by the two-step sequential deprotonation and metal coordination route lead to the formation of a mixture of products with ligand **2**, whereas no complexes at all could be identified when ligands **3** and **4** were used. This outcome may be related to the inherent instability of the respective free carbenes, when containing small alkyl *N*-substituents,[25–27] though accessibility of these free carbenes has been demonstrated.[28–31] Complex formation was also unsuccessful when applying a one pot synthesis using equimolar quantities of imidazolium salt and $Cu(OAc)_2$ in the presence of *t*BuOK (1.2 molequiv.) under inert conditions (dry THF, N_2 atmosphere). These experiments demonstrate the significant

advantages of the decarboxylation route, especially when the free carbene is highly unstable such as the dimethyl-substituted NHC **4**.

Scheme 2. Synthesis of complexes (**1–4**)$Cu(OAc)_2$ following the decarboxylation route, using ligands (**1–4**)-$\mathbf{CO_2}$.

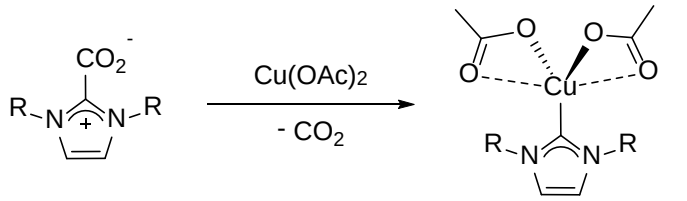

	R	
1-CO_2	2,6-diisopropylphenyl	(**1**)$Cu(OAc)_2$
2-CO_2	mesityl	(**2**)$Cu(OAc)_2$
3-CO_2	isopropyl	(**3**)$Cu(OAc)_2$
4-CO_2	methyl	(**4**)$Cu(OAc)_2$

Variation of the anion in (NHC)Cu(X)$_2$ complexes. The versatility of the decarboxylation route was further demonstrated by metalating ligand **1-CO_2** with various sources of Cu including $CuCl_2$, $CuBr_2$, $Cu(NO_3)_2$•x H_2O, and $Cu(BF_4)_2$•x H_2O (Scheme 3). All complexes (**1**)CuX_2 were synthesized also by the deprotonation route starting from **1H.Cl** for comparative purposes. Complexes (**1**)$CuCl_2$, (**1**)$CuBr_2$, (**1**)$Cu(NO_3)_2$•2 H_2O, and (**1**)$Cu(BF_4)_2$ were isolated by Et_2O precipitation as microanalytically pure solids following both routes. We note that water molecules are only found with the nitrate complex (**1**)$Cu(NO_3)_2$•2 H_2O, irrespective of the synthetic route used, which may be due to water coordination to the copper center, [(**1**)$Cu(H_2O)_2$]$(NO_3)_2$, or the formation of a dihydrate of (**1**)$Cu(NO_3)_2$. All other complexes were water-free according to elemental analysis, indicating that the use of reagent-grade moist solvents for the decarboxylation route did not induce coordination of water to the copper center. In contrast, reaction with $Cu(OTf)_2$ afforded a sticky solid that did not provide any evidence for Cu-NHC complex formation.

Scheme 3. Synthesis of complexes (**1**)CuX_2 following the decarboxylation route using **1-CO₂**, with X = OAc, Cl, Br, BF_4 or NO_3.

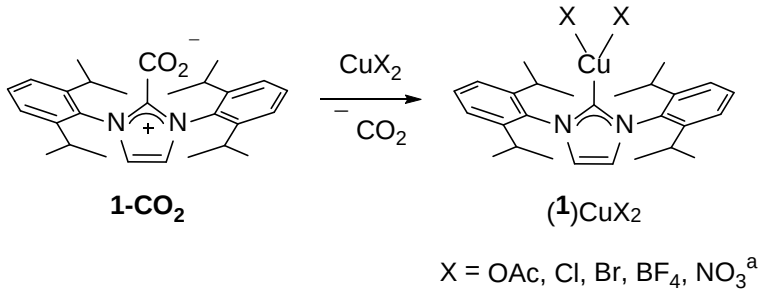

[a] According to elemental analysis, contains two molecules of water, either coordinated to the Cu ion or as non-coordinated hydrates.

IR analysis of the complexes (**1–4**)$Cu(X)_2$ (X = OAc, Cl, Br, BF_4 or NO_3) supported the successful decarboxylation as the prominent vibration bands attributed to the carboxylate group of the ligand precursors (**1–4**)**-CO₂** were absent (Fig. S2–S6). Moreover, the IR spectra of the complex prepared via the decarboxylation route were essentially identical to those of samples prepared by the deprotonation route. Mass spectrometry of the respective solids dissolved in acetonitrile did not show any signal related to the carboxylate ligand, as exclusively $[(NHC)Cu(MeCN)]^+$ fragment ions (see Fig. S14-15) were observed when analysing (**1**)CuX_2 (X = Cl or Br). Indeed, the observation of the $[(NHC)Cu(MeCN)]^+$ fragment confirmed the successful formation of the $Cu–C_{NHC}$ bond.

UV-vis spectroscopic analyses. Light blue solutions of each of the complexes (**1–4**)$Cu(OAc)_2$ dissolved in CH_2Cl_2 were studied by absorption spectroscopy. All complexes exhibit a very strong absorbance in the UV region, attributed to ligand π–π* transitions, and a weak band in the vis-NIR domain which was assigned to Cu(II) d–d transitions (Figure 4, Table 1). The d–d transition bands display a shoulder at lower energy which is characteristic for a square-pyramidal metal coordination geometry at copper.[32] The maximum wavelength in the 660–695 nm range and the molar absorptivity values (70–105 cm^{-1} M^{-1}) are typical for d–d transitions in Cu(II) complexes, yet the broad character of the band does not allow any trend to be deduced.

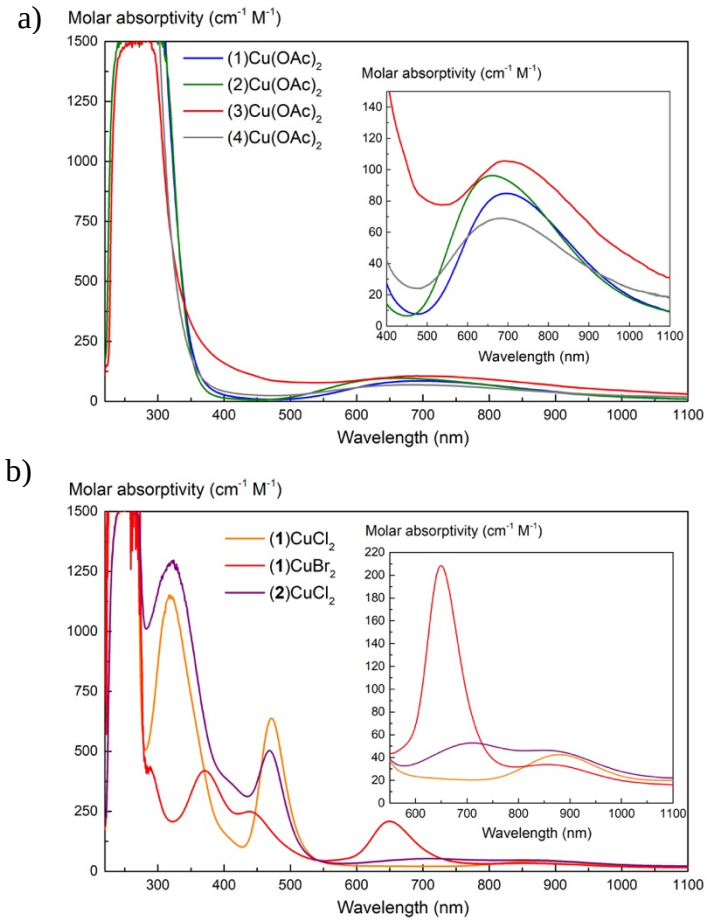

Figure 4. UV-vis-NIR absorption spectra of a) complexes series (NHC)Cu(OAc)$_2$ and b) complexes (**1**)CuCl$_2$, (**1**)CuBr$_2$ and (**2**)CuCl$_2$ at 1 mM in CH_2Cl_2. Complexes [(**1**)Cu(OH$_2$)$_2$](NO$_3$)$_2$ and (**1**)Cu(BF$_4$)$_2$ did not give clear solutions for UV-vis measurement.

Table 1. Spectrophotometric data observed for the complexes in solution.

Complex	λ_{max} (nm)	ε (cm^{-1} M^{-1})	Band width (nm)[a]
(**1**)Cu(OAc)$_2$	694	85	317
(**2**)Cu(OAc)$_2$	662	95	316
(**3**)Cu(OAc)$_2$[b]	690	105	406
(**4**)Cu(OAc)$_2$	682	70	378
(**1**)CuCl$_2$	471	640	46
	880	45	273
(**1**)CuBr$_2$	437	250	94
	649	210	80
	855	35	410
(**2**)CuCl$_2$	468	500	54
	709	55	304
	849	45	410

[a] band width determined as full width at half maximum. [b] Solution was turbid.

The UV-vis absorption characteristics of the Cu(II) complexes (**1**)CuX_2 are strongly dependent on the nature of the anion X^-. While all complexes display intense ligand π–π* transitions in the UV region, complex (**1**)$CuCl_2$ features additionally a substantial band at 471 nm and a weak absorption in the NIR range around 880 nm, which was attributed to Cu(II) d–d transitions (Figure 4, Table 1). Complex (**1**)$CuBr_2$ has a much stronger absorption at 649 nm with a shoulder at lower energy (855 nm) that is similar to the absorption properties of complex (**1**)$CuCl_2$ (Table 1). Notably, complexes [(**1**)$Cu(OH_2)_2$]$(NO_3)_2$ and (1)$Cu(BF_4)_2$ did not give clear solutions for reliable UV-vis spectroscopic analysis.

The role of the anion X^- for defining the UV-vis characteristics is further underlined by the analytical data of complex (**2**)$CuCl_2$. This complex was prepared via decarboxylation of **2-CO₂** with $CuCl_2$ (*cf* Fig. S7 for IR characterization) and displays UV-vis properties similar to (**1**)CuCl2, in particular a weak absorption band in the NIR range around 870 nm with a similar extinction coefficient (*ca*. 40 cm^{-1} M^{-1}). These similarities indicate that the nature of the halide is relevant for defining the d-d transition, while the type of NHC ligand (**1** *vs* **2**) plays a less prominent role.

EPR spectroscopic analyses. The EPR spectrum of a frozen solution of complex (**1**)$Cu(OAc)_2$ in CH_2Cl_2/toluene is approximately axial with $g_{//}>g_{\perp}>2.003$ ($g_{//} = g_1$ and $g_{\perp} = g_2 = g_3$), typical for square-pyramidal Cu(II) geometries with a $d_{x^2-y^2}$ ground state (Figure 5),[33] and in good agreement with the UV-vis spectroscopic analyses (*vide supra*). It is considerably different from pure $Cu(OAc)_2$ (see below) or a mixture of $Cu(OAc)_2$ and imidazolium salt **1H.Cl** (featureless spectrum), which were measured as controls. The spectrum of $Cu(OAc)_2$ displays a resolved but rather weak $g_{\perp}$ signal around 2.07, while the spectrum of the mixture of $Cu(OAc)_2$ and **1H.Cl** was featureless and no signal was resolved. The spectrum of (**1**)$Cu(OAc)_2$ is identical irrespective of the applied synthetic methodology (deprotonation *vs* decarboxylation) and therefore supports the suitability of decarboxylation to form a Cu(II)–C_{NHC} bond (vide infra). The signals were notably broadened, which was attributed to a mixture of two species in solution, possibly due to variations in the coordination modes of the acetate ligands.[34] The splitting of the signal at low field (2750 G) has been attributed to partially separated ^{63}Cu and ^{65}Cu absorptions from a $Cu(OAc)_2$ spectrum.[35] The spectrum was simulated with EasySpin, using two isomers with slightly deviating parameter sets, {$g_1 = 2.290$, $g_2 = g_3 = 2.055$, $A_1(^{63}Cu) = 160 \times 10^{-4}$ cm^{-1}} and {$g_1 = 2.280$, $g_2 = g_3 = 2.055$, $A_1(^{63}Cu) = 185 \times 10^{-4}$ cm^{-}

^{1}} (Figure S17). The parameters determined for (**1**)Cu(OAc)$_2$ are different from those previously reported for Cu(II) complexes with chelating NHC ligands (Table 2). For example, Meyer's tris-NHC Cu(II) complex **D** (*cf* Fig. 1) has a tetrahedral geometry and displays a rhombic signal with similar g values and a lower hyperfine coupling constant.[8] Bis-alkoxy-NHC Cu(II) complexes akin to complex **C** (*cf* Fig. 1) have been reported by Arnold et al. with smaller g_1 and a broad range of A_1 values.[7] However, the EPR data for complex (**1**)Cu(OAc)$_2$ represent the first data set for a Cu(II) complex with a monodentate NHC ligand.

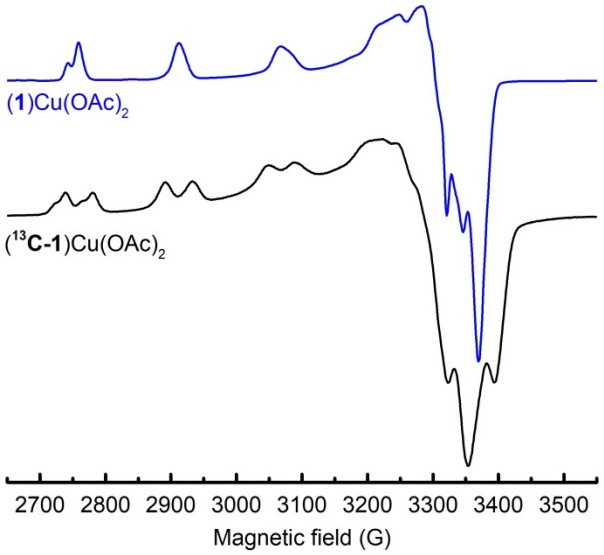

Figure 5. X-band EPR spectra at 77 K of complexes (**1**)Cu(OAc)$_2$ (blue line) and (**^{13}C-1**)Cu(OAc)$_2$ (black line) in CH_2Cl_2:toluene 1:9; comparative spectra for (**1**)Cu(OAc)$_2$ in DMF/toluene are shown in Fig. S19.

Table 2. EPR parameters of the different (NHC)CuX$_2$ complexes.[a]

Spin Hamiltonian parameters	g_1	g_2	g_3	A_1 (^{63}Cu)[b]	A_2 (^{63}Cu)[b]	A_3 (^{63}Cu)[b]
(**1**)Cu(OAc)$_2$	2.290	2.055	2.055	160	0	0
(**2**)Cu(OAc)$_2$	2.290	2.075	2.035	160	20	0
(**3**)Cu(OAc)$_2$	2.375	2.058	2.058	165	20	0
(**4**)Cu(OAc)$_2$	2.378	2.050	2.035	167	20	0
(**1**)CuCl$_2$	2.365	2.072	2.043	122	0	0
[(**1**)Cu(H$_2$O)$_2$](NO$_3$)$_2$	2.285	2.057	2.050	135	38	0
(**1**)Cu(OAc)$_2$'	2.280	2.055	2.055	185	0	0
(**2**)Cu(OAc)$_2$'	2.266	2.075	2.035	175	20	0
(**3**)Cu(OAc)$_2$'	2.315	2.058	2.038	180	20	0
(**4**)Cu(OAc)$_2$'	2.321	2.050	2.035	170	20	0
[(TIMEN^{Bz})Cu](OTf)$_2$[8]	2.275	2.060	2.005	132	0	0
[Cu(L)$_2$]•2(LiI)[7]	2.10–2.16	1.97–2.05	1.95–2.043	100-202[c]		

[a] X = OAc, Cl, Br, BF_4, NO_3; all values are extracted from EasySpin simulation of spectra recorded in DMF/toluene (1:9) at 77 K. [b] Unit for hyperfine parameter is 10^{-4} cm^{-1}. [c] Unit is reported as G.

To establish the carbene hyperfine coupling constant in Cu(II)-NHC complexes, the ^{13}C-labelled ligand **^{13}C-1H.Cl** was synthesized[36] and complex (**^{13}C-1**)Cu(OAc)$_2$ was isolated upon reaction with *t*BuOK and Cu(OAc)$_2$. While elemental analysis, mass spectrometry and powder X-Ray diffraction analyses of crystals of (**^{13}C-1**)Cu(OAc)$_2$ are identical with those of the non-labelled complex (**1**)Cu(OAc)$_2$ (*cf* experimental part and Fig. S1), EPR spectroscopy shows distinct differences (Figure 5). The hyperfine signals splitting is especially clear in the $g_{//}$ region, with a simulated coupling constants $a(^{13}C)_1 = 44 \times 10^{-4}$ cm^{-1} (Figure S18). Moreover, this large coupling constant unambiguously confirms the formation of a C_{NHC}–Cu bond. In addition, the EPR data provide support for the integrity of (**1**)Cu(OAc)$_2$ in solutions used for EPR spectroscopy (CH_2Cl_2/toluene and DMF/toluene, Fig. S19).

Variation of the NHC ligand in complexes (**1–4**)Cu(OAc)$_2$ revealed some general features (Figure 6). (**1–4**)Cu(OAc)$_2$ exhibit rhombic EPR spectra in DMF/toluene with signals at g_2, g_3 = 2.03–2.08, and the characteristic ^{63}Cu hyperfine splitting in the $g_1 \approx 2.3$, which was not observed in the spectrum of Cu(OAc)$_2$ and therefore supports complex formation. The broadening and splitting of the signals in the EPR spectra of (**1–4**)Cu(OAc)$_2$ were reproduced in the simulated spectra only when considering the spectra as a mixture of two species, which are probably induced by mono- or bidentate acetate coordinating in solution. For convenience, the species with the set of lower field g values is denoted here as (**1–4**)Cu(OAc)$_2$ and the one with higher field values as (**1–4**)Cu(OAc)$_2$'.

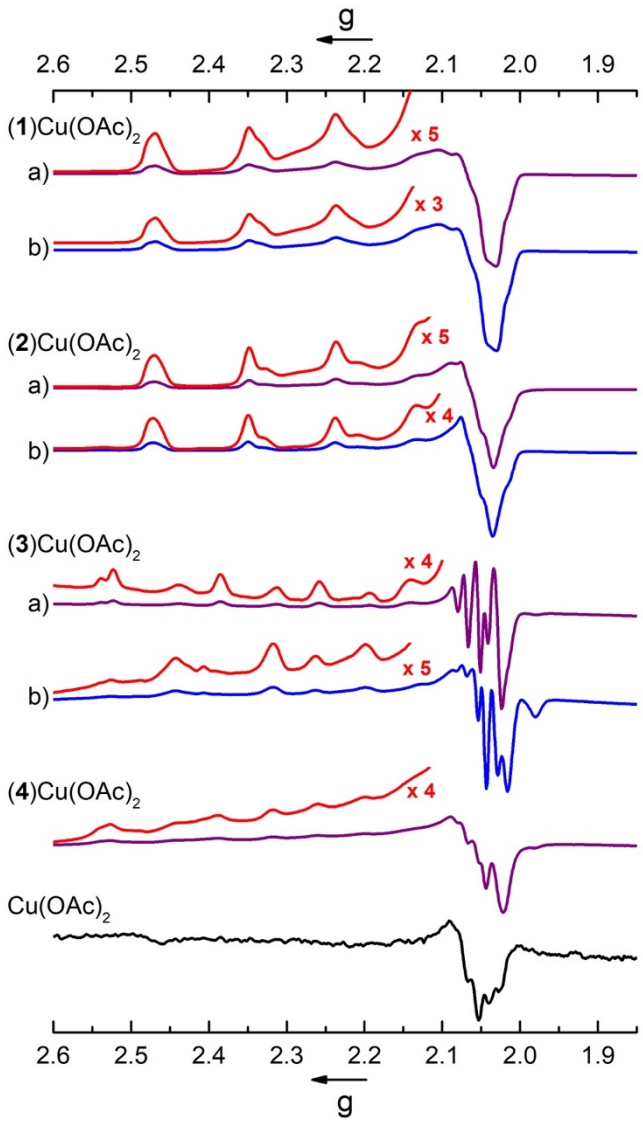

Figure 6. X-band EPR spectra at 77 K of frozen solution of $Cu(OAc)_2$ (bottom black line) and the reaction mixtures in DMF/toluene (1:9) of the products from (a) decarboxylation of (**1–4**)**–CO₂** (purple lines) and from (b) deprotonatation of the imidazolium salt (**1–3**)**H.X** (blue lines) in the presence of $Cu(OAc)_2$ that yield complexes (**1-4**)$Cu(OAc)_2$. The insets (red lines) show an expansion of the Cu hyperfine coupling in the g_1 area. For **3-CO₂** and **4-CO₂**, solution in DMF:toluene 1:9 of the resulting isolated solid.

The nature of the NHC ligand directly affects the spin Hamiltonian parameters (Table 2, *cf* Figures S19-S22 for simulated spectra and full list of parameters). With decreasing bulkiness and increasing donor properties of the N-wingtip groups from aryl to alkyl derivatives, the g_1 values increase from 2.27–2.29 to 2.32–2.38 for complexes (**1–2**)$Cu(OAc)_2$ *vs* (**3–4**)$Cu(OAc)_2$ and also the hyperfine splitting constant A_1 increases (160 to 167 x 10^{-4} cm^{-1}). The same trend is observed for the g_1 value of the second species (**1–4**)$Cu(OAc)_2$', however with decreasing A_1 values (185 to 170 x 10^{-4} cm^{-1}). Moreover, modification of the NHC reduces the difference of the g_1 values between the high and low field species (from 0.06 to 0.01 with NHC variation

from **4** to **1**). The difference in g_1 and A_1 values with variation of the bulkiness of the NHC ligand suggests a change in geometry of the complexes in solution. Specifically, binding of the second acetate oxygen may be influenced by H-bonding interactions, as deduced from the close contact of the oxygen with the CMe_2–H hydrogen of the aryl wingtip group in the crystal structure of (**1**)$Cu(OAc)_2$ (C–H….O = 2.609 Å).[12]

EPR spectra of the reaction mixtures from decarboxylation of **1–CO₂** with different CuX_2 precursors gave diverging results that depend on the anion X^- in the Cu source (Figure 7; *cf* Figures S23-S25 for simulated spectra and full list of parameters). The spectra were featureless for $CuBr_2$ and $Cu(BF_4)_2$ and the corresponding complexes (**1**)$CuBr_2$ and (**1**)$Cu(BF_4)_2$, which might be a consequence of reduction of the metal center to Cu(I) (S = 0) or because of magnetic interactions between the Cu(II) centers that induce broadening of the signals.[37] In contrast, the spectrum of (**1**)$CuCl_2$ displays approximate axial symmetry with a broad resonance at $g_1 = 2.36$ ($A_1 = 122 \times 10^{-4}$ cm^{-1}) and a signal at $g_3 = 2.04$ without a detectable hyperfine splitting (Table 2). These features are distinct from those of the $CuCl_2$ precursor, which shows hyperfine splittings at $g_1 = 2.35$ ($A_1 = 121 \times 10^{-4}$ cm^{-1}) and $g_3 = 2.00$ ($A_3 = 64 \times 10^{-4}$ cm^{-1}), which support Cu(II)–NHC bond formation when starting from $CuCl_2$. The broadness of the signals of (**1**)$CuCl_2$ is characteristic for Cl^- bound to copper, and is also observed for complex (**2**)$CuCl_2$ (*cf* Fig. S26). The spectra of $Cu(NO_3)_2$ and $Cu(OTf)_2$ were measured from hydrated salts, and thus display the same $g_1 = 2.40$ and $A_1 = 137 \times 10^{-4}$ cm^{-1} values for $[Cu(OH_2)_4]^{2+}$.[38] When complexed by the NHC **1**, the nitrate complex features a less resolved hyperfine splitting at $g_1 = 2.29$ ($A_1 = 135 \times 10^{-4}$ cm^{-1}) and new signals at $g_2 = 2.06$ ($A_2 = 38 \times 10^{-4}$ cm^{-1}) corroborate NHC bonding to the Cu(II) center. In contrast, the reaction mixture containing the deprotonated ligand **1** and $Cu(OTf)_2$ shows the same signals as pure $Cu(OTf)_2$, which suggests no significant interaction between the carbene and $Cu(OTf)_2$.

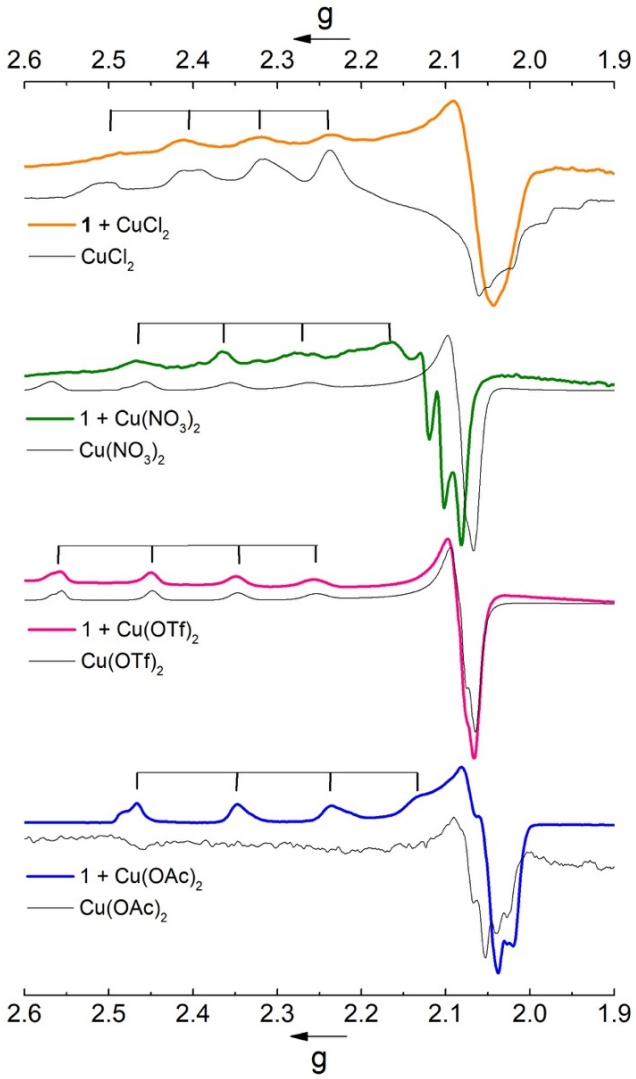

Figure 7. X-band EPR spectra at 77 K of frozen solution of Cu salts (black lines) and the reaction mixtures in DMF/toluene (1:5) of the deprotonated ligand **1** and the corresponding Cu salt; the identity of the spectra of $Cu(OTf)_2$ with or without NHC ligand **1** suggest no significant complex formation.

NMR spectroscopy and other solution state considerations of complexes (1–4)Cu(OAc)$_2$. Finally, our investigations also included ^{1}H NMR spectroscopy of a solution of (**1–4**)$Cu(OAc)_2$ in CD_2Cl_2. As expected, broad signals characteristic of paramagnetic effects were observed in the 0–12 ppm range (Figure S27). While allocation of signals was not trivial, the larger than expected number of signals suggests the co-existence of different isomers or aggregates, in agreement with the EPR measurements. Diffusion ordered spectroscopy (DOSY) experiments were performed to distinguish between different aggregate sizes. Actually, the diffusion constants of the various species appeared essentially identical and did not lead to a clear separation of species (Figure S28, Table S3). This similarity suggests only minor changes, *e.g.*, imparted by mono- vs bidentate bonding of the acetate ligand. The $^{13}C\{^1H\}$ NMR spectra did not show any resonance that is attributable to the CO_2 group (δ_C = 152 for ligand precursor **1-**

CO_2) and hence support successful decarboxylation *en route* to the formation of the (NHC)$Cu(OAc)_2$ complex (Figure S29).

Similarly, NMR spectroscopic analyses of complexes (**1**)$CuCl_2$ and (**1**)$CuBr_2$ dissolved in CD_2Cl_2 revealed only broad signals in the ^1H NMR spectra characteristic for paramagnetic species (Figures S30–31). Therefore, UV-vis and NMR analyses of (**1**)$CuBr_2$ strongly suggest the formation of a Cu(II)-NHC complex, even though this complex is EPR silent as a solid or in frozen solution at 77 K. In contrast, sharp signals were noted in the NMR spectra of complexes [(**1**)$Cu(OH_2)_2$]$(NO_3)_2$ and (**1**)$Cu(BF_4)_2$, which are identical to those of the protonated imidazolium salt $\mathbf{1H^+}$, suggesting that the complexes decomposed in solution (Figure S32). While EPR measurements and elemental analysis support formation of the nitrate complex [(**1**)$Cu(OH_2)_2$]$(NO_3)_2$, the formation of (**1**)$Cu(BF_4)_2$ is only supported by elemental analysis. No support has been obtained for the formation of the carbene complex with triflate ions. Despite these limitations, the analytical data indicate that the decarboxylation route is useful for the preparation of a variety of (NHC)CuX_2 complexes without taking precautions about the presence of air or moisture. The synthetic procedure is versatile and tolerates variability both in the NHC ligand (alkyl, aryl substituents on nitrogen, **1**–**4**) and in the complex anion (Cl, Br, OAc, NO_3).

Reassembling and reorganization patterns. Pure and isolated complexes (**1–4**)CuX_2 are not stable when re-dissolved and rearrange *e.g.* upon re-crystallization, a behaviour that is typical for copper complexes and strongly dependent on both reaction conditions (concentration, reaction temperature) and the nature of the ligands and anions. Crystallization was typically induced by slow diffusion of Et_2O into a concentrated solution of the respective Cu(II) complex in CH_2Cl_2. Single crystal X-ray diffraction analysis of these crystals revealed structures that are distinctly different from the formulations deduced by elemental and spectroscopic analysis performed directly after complex formation. It is noteworthy that complex (**1**)$Cu(OAc)_2$ repeatedly yielded a well-defined molecular structure with a trigonal planar Cu(II) center as reported earlier,[12] i.e. the combination of carbene **1** and two acetate anions provides a stable geometry of the Cu(II) cation. However, slight variation of both the NHC and the anionic ligand X^- induced rearrangements upon crystallisation that entail either heterolytic Cu–NHC bond scission or homolytic Cu–X bond cleavage. The prevailing type of rearrangement is dictated by ligand pattern as outlined below.

Dissociation of the Cu–NHC bond was observed upon crystallization of complexes (**3**)Cu(OAc)$_2$ and (**4**)Cu(OAc)$_2$. These complexes rearrange to an acetate cuprate as complex anion that is charge balanced by imidazolium cations. Crystals stemming from NHC dissociation from complex (**3**)Cu(OAc)$_2$ reveal a polymeric copper acetate anion composed of $[Cu_2(OAc)_5]^-$ monomer units with paddlewheel $Cu_2(OAc)_4$ clusters linked by a bridging κ^2,μ^2-bound acetate ligand (Figure 8). The C2-bound hydrogen of the imidazolium cation **3H**$^+$ features short distances in the 3.1–3.5 Å range to oxygen atoms of several acetates, which indicates significant hydrogen bonding (Figure S33).

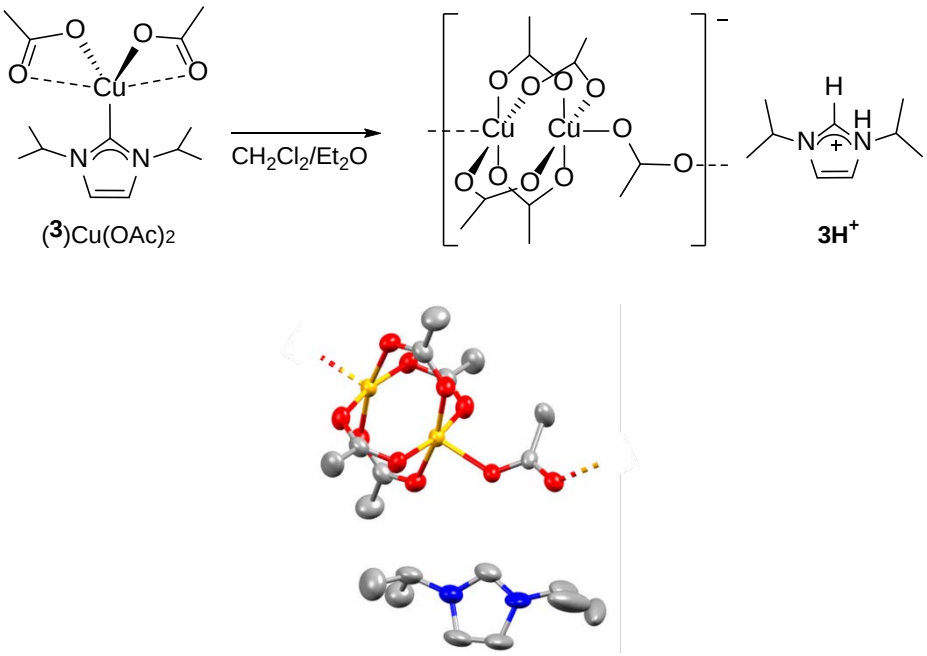

Figure 8. Top, reaction scheme of the re-assembly of (**3**)Cu(OAc)$_2$ into (**3H**)[Cu$_2$(OAc)$_5$]; for clarity, the delocalised π electrons of the acetate ligands has been omitted in the schematic respresentation of the Cu$_2$(OAc)$_4$ cluster. Bottom, ORTEP representations of (**3H**)[Cu$_2$(OAc)$_5$]. (50% probability ellipsoids; hydrogen atoms and solvent molecules omitted for clarity).

The rearrangement of complex (**4**)Cu(OAc)$_2$ is very similar, however the copper acetate complex anion is composed of alternating paddlewheels Cu$_2$(OAc)$_4$ cluster and monomeric Cu(OAc)$_2$ units, both linked with a bridging κ^2,μ^2-bound acetate ligand, indicating versatility of the Cu(OAc)$_n$ synthon (Figure 9). Again, significant hydrogen bonding is present between the protons of the imidazolium cation **4H**$^+$ and the acetate oxygen atoms (Figure S34). Similar copper carboxylate polymers were previously described, though with different linkers such as bridging 4-4'-bipyridine,[39,40] or alternate with Cu(II) complexes such as (1,10-phenanthroline)Cu motifs.[41] Also tetrametallic systems were reported that contain one paddlewheel cluster linked to two Cu(carboxylate)$_2$ motifs similar to the complex anion resulting from rearrangement of (**4**)Cu(OAc)$_2$, yet terminated by water molecules.[42]

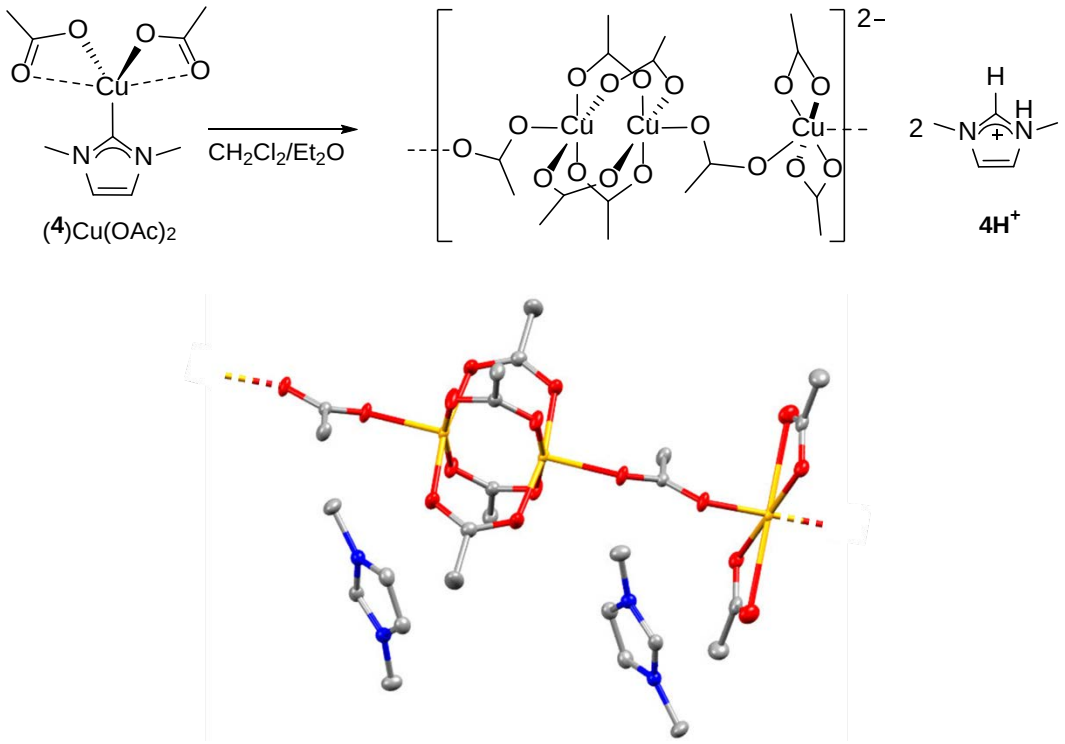

Figure 9. Top, reaction scheme of the re-assembly of (**4**)Cu(OAc)$_2$ into (**4H**)$_2$[Cu$_3$(OAc)$_8$]; for clarity, the delocalised π electrons of the acetate ligands has been omitted in the schematic respresentation of the Cu$_3$(OAc)$_8$ cluster. Bottom, ORTEP representations of (**4H**)$_2$[Cu$_3$(OAc)$_8$] (50% probability ellipsoids; hydrogen atoms and solvent molecules omitted for clarity).

Disproportionation occurred as a different rearrangement pathway for complex (**2**)Cu(OAc)$_2$ containing a more stable aryl substituted NHC ligand. Under crystallization conditions, this complex transformed to a bis(imidazolylidene) Cu(I) complex cation [(**2**)$_2$Cu]$^+$ charge balanced by a molecularly discrete monoanionic and bimetallic cuprate cluster [Cu$_2$(OAc)$_5$(HOAc)]$^-$ (Figure 10). The Cu(I)–C$_{NHC}$ bond lengths of 1.880 and 1.883 Å are similar to the bond lengths measured in previously reported complexes [(**2**)$_2$Cu](X) (X = BF$_4$, PF$_6$), synthesized by reaction between the deprotonated ligand and a Cu(I) source.[43] The [(**2**)$_2$Cu]$^+$ copper(I) ion was also identified by mass spectrometry with a signal at m/z 671.3188 (calc. 671.3175) from a MeCN solution of the isolated powder of (**2**)Cu(OAc)$_2$ (Fig. 10–11). Of note, a frozen solution of the crystals was EPR silent, which is expected for a Cu(I) salt and Cu(II) acetate clusters,[44,45] yet in marked contrast to the behaviour of the complex before crystallization (*cf* Figure 6).

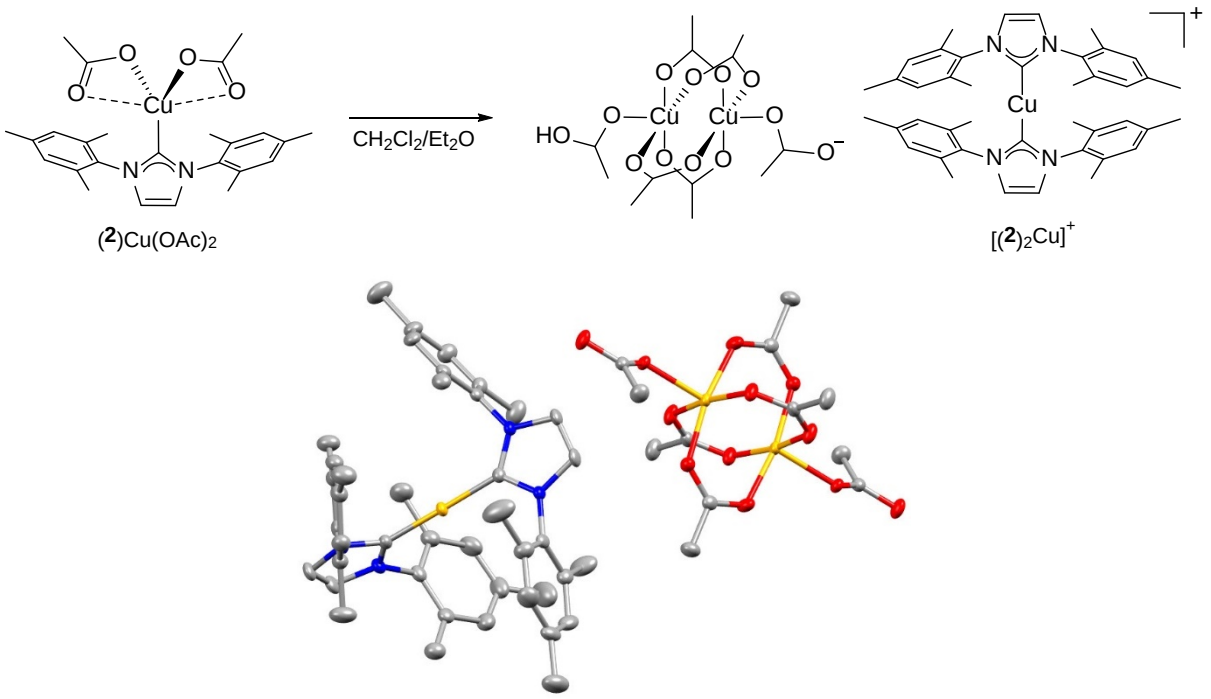

Figure 10. Top, reaction scheme of the re-assembly of (**2**)$Cu(OAc)_2$ into [(**2**)$_2$Cu][$Cu_2(OAc)_5(HOAc)$]. Bottom, ORTEP representation of [(**2**)$_2$Cu][$Cu_2(OAc)_5(HOAc)$] (50% probability ellipsoids; hydrogen atoms and solvent molecules omitted for clarity).

Crystallization of (**1**)$CuBr_2$, afforded co-crystals of imidazolium dibromocuprate in which the imidazolium cation is either brominated at C2 position or protonated, *i.e.* **1Br.CuBr2** and **1H.CuBr2**. The refinement converged at a 87:13 ratio of the two cations, and also the $CuBr_2^-$ anion is disordered in the same proportion, indicating that each cation has its specific anion (Figure 11). The formation of **1Br.CuBr2** is further supported by a mass spectrometry signal in positive ionization mode at m/z 467.2051 (calc. for **1Br**$^+$ 467.2062) from a MeCN solution of the powder of (**1**)$CuBr_2$ (Fig. S15).

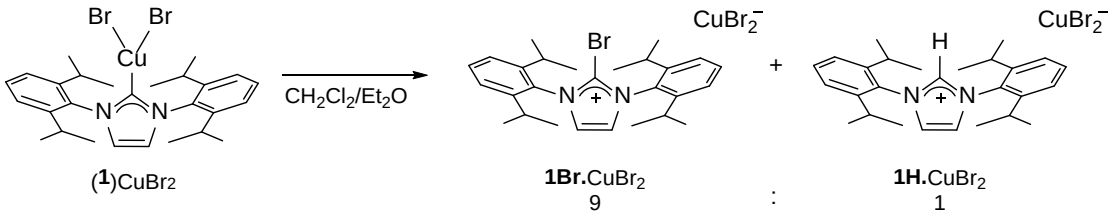

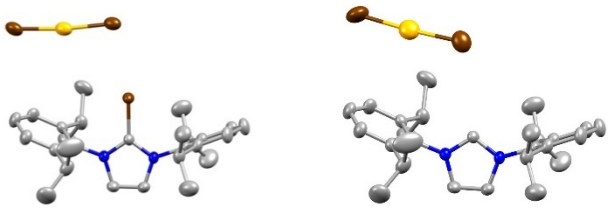

Figure 11. Re-assembly of (**1**)$CuBr_2$ into **1Br.CuBr$_2$** and **1H.CuBr$_2$** and ORTEP representations of the two co-crystallized salts with a refined weighting of 87% **1Br.CuBr$_2$** and 13% **1H.CuBr$_2$** (50% probability ellipsoids; hydrogen atoms omitted for clarity).

A similar transformation was observed under crystallization conditions when starting from the chloro analogue (**1**)$CuCl_2$. While mass spectrometry identified the 2-chloroimidazolium cation **1Cl$^+$** (m/z 423.2540, calc. 423.2567) (Fig. S14), single crystals grown from the mixture only showed the protonated imidazolium salt **1H.CuCl$_2$** (Scheme 4). A unit cell determination was identical with the previously reported structure of this compound synthesized from **1H.Cl** and CuCl.[46]

Scheme 4. Reaction scheme of the re-assembly of (**1**)$CuCl_2$ into **1Cl.CuCl$_2$** and **1H.CuCl$_2$**.

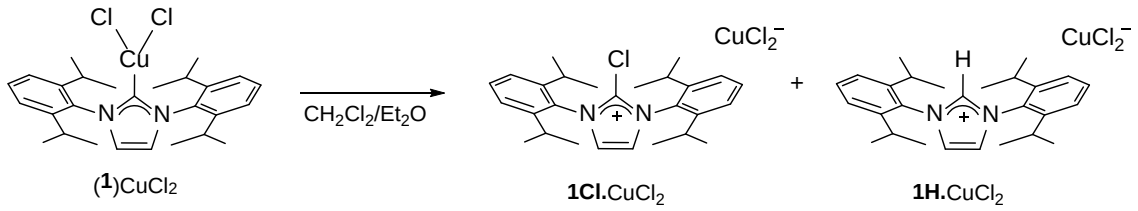

These re-assembly patterns suggest some general reactivity trends for Cu(II)-NHC complexes featuring (i) Cu–NHC bond dissociation and (ii) disproportionation of the Cu(II) complexes, which may induce reductive elimination pathways (Scheme 5). The selectivity is governed by the stability of the carbene as well as the nature of the anion X in the Cu(II) complexes. Thus, complexes bearing acetate and relatively unstable *N*-alkylated NHCs such as **3** or **4**, undergo Cu(II)-NHC bond dissociation, presumably imparted by the weak Cu–C_{NHC} bond in these complexes (left side of Scheme 5). For poorly stabilized free carbenes, protonation by residual water makes the dissociation irreversible and induces the assembly of copper acetate units into different types of structural motifs, presumably templated by hydrogen bonding.

With more stable NHCs such as the *N*-aryl substituted ligand **2**, such bond dissociation may be reversible and instead, a disproportionation pathway is proposed to occur, which involves homolytic Cu–OAc bond cleavage through a dimeric Cu(II)-Cu(II) species (right side of Scheme 5). This disproportionation yields [(**2**)Cu^{I}(OAc)] and [(**2**)$Cu^{III}(OAc)_3$] as unobserved

intermediates. Based on hard-soft considerations, the Cu–OAc bond in the cuprous salt is expected to be much less stabilized than in the cupric precursor, and therefore leads to the formation of the bis(carbene) Cu(I) complex. The second NHC ligand is presumably originating either from transient NHC dissociation from the Cu(II) precursor complex (*cf* left side of Scheme 5), or by a ligand scrambling process between two molecules of (**2**)Cu(OAc) as established for NHC–Ag(I) complexes.[47] In such a model, the cuprate anion may be formed via H-atom abstraction by the unstable Cu(III) salt originating from the disproportionation reaction, which then rearranges into the anionic paddlewheel Cu(II) acetate cluster.[44] Accordingly, the distinct rearrangement of (**2**)$Cu(OAc)_2$ is associated with the less basic and more stable nature of the carbene when substituted with bulky aryl wingtip groups. NHC dissociation leads then to a free carbene that is sufficiently long-lived for re-coordination to a copper center, preferably to soft Cu(I), rather than being protonated as observed in the rearrangement of (**3**)$Cu(OAc)_2$ and (**4**)$Cu(OAc)_2$. In agreement with this model, the bulkiest and most stable carbene of the series, *viz.* **1**, does not undergo any detectable NHC protonation and complex (**1**)$Cu(OAc)_2$ is stable. Hence, stability effects imparted by the NHC wingtip group trigger the course of ligand re-assembly. Less bulky and less stable NHCs induce a more labile NHC–Cu bond and lead to carbene reshuffling or even carbene protonation.

In the presence of a bromide or chloride anions rather than acetate, both pathways are observed. NHC–Cu dissociation affords the imidazolium cations $\mathbf{1H^+}$, while disproportionation is evidenced by the formation of the imidazolium cations $\mathbf{1Cl^+}$ and $\mathbf{1Br^+}$. Disproportionation as discussed for (**2**)$Cu(OAc)_2$ leads to a mixture of (**1**)CuBr and (**1**)$CuBr_3$ when starting from (**1**)$CuBr_2$. While reductive NHC–OAc elimination is prevented, reductive elimination from (**1**)$CuBr_3$ is well conceivable and produces the brominated imidazolium cation $\mathbf{1Br^+}$ together with the dibromo cuprate anion as $\mathbf{1Br.CuBr_2}$. This reaction pathway is supported by the fact that the cation $\mathbf{1Br^+}$ was previously synthesized from the Cu(I) complex (**1**)CuBr in the presence of an oxidant through the formation of a putative Cu(III)-NHC tris(halide) complex.[48] The similarity of product formation for the bromide and chloride complexes suggests that the disproportionation and reductive elimination is a rather general pathway for copper re-assembly with halides and likely with other anions that are susceptible to reductive C–X bond formation.

Scheme 5. Reaction scheme of the different reactivity trends of the reassembly of complex (**NHC**)CuX_2, depending on the nature of the carbene and the anion.

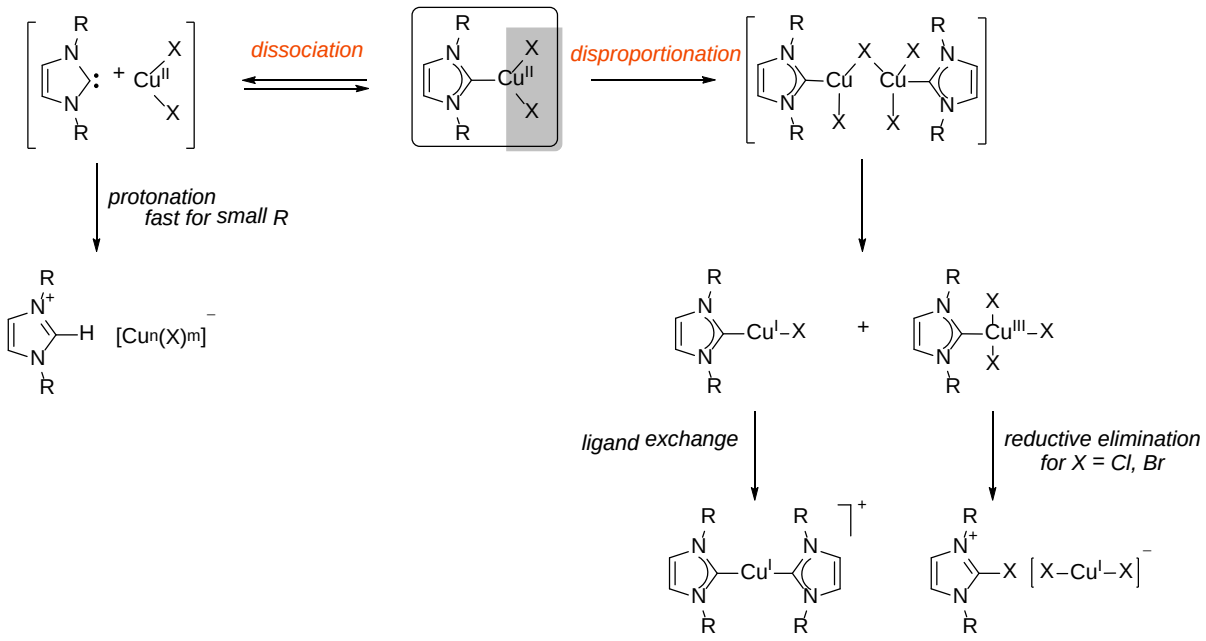

Conclusions

Herein, we have demonstrated the suitability of the decarboxylation process for the preparation of NHC Cu(II) complexes using imidazolium carboxylate precursors. This methodology does not require the use of inert conditions and allows to extend the family of monodentate NHC Cu(II) complexes to include carbenes such as 1,3-dimethylimidazolylidene, which are inherently unstable and therefore difficult to be metalated by a free carbene route. The loss of the carboxylate group from the imidazolium carboxylate precursor and the formation of complexes of identical structures following either the free carbene or the decarboxylation route demonstrate that Cu(II) binds to the NHC ligand to generate complex (NHC)$Cu(X)_2$ as efficiently but without the need for inert conditions and more directly than when following the reported two-step deprotonation route. A variety of Cu(II) salts were successfully used to study the influence of the anion on the stability of the complexes. Further spectroscopic characterization of Cu(II)-NHC complexes led to the first determination of carbene-Cu hyperfine coupling constant by EPR spectroscopy of a specifically ^{13}C-labeled complex (**^{13}C-1**)$Cu(OAc)_2$. The unsupported Cu(II)-NHC complexes are prone to rearrangement and further reaction under re-crystallisation conditions. Specific cleavage patterns were identified, including heterolytic Cu–NHC bond dissociation when the free NHC is unstable, as well as homolytic Cu–X bond cleavage (for X = OAc, Br, Cl). The distinct patterns imparted by the

ligand set bound to the Cu(II) center have direct implications for application of such complexes, *e.g.* in homogeneous catalysis.

Experimental section

Materials and methods. All reagents were commercially available and used as received from Sigma-Aldrich or Acros. NMR spectra were recorded at 25 °C on Bruker spectrometers operating at 300 or 400 MHz (^{1}H NMR), and 75 MHz (^{13}C NMR), respectively. Chemical shifts (δ in ppm, coupling constants J in Hz) were referenced to residual solvent signals (^{1}H, ^{13}C). Assignments are based on homo- and heteronuclear shift correlation spectroscopy. Purity of bulk samples of the complexes has been established by mass spectroscopy and elemental analysis. Elemental analyses were performed at DCB Microanalytic Laboratory using a Thermo Scientific Flash 2000 CHNS-O elemental analyzer. High-resolution mass spectrometry was carried out with a Thermo Scientific LTQ Orbitrap XL (ESI-TOF) by the mass spectroscopy group of the Department of Chemistry and Biochemistry, University of Bern, PD Dr. S. Schürch. The solid were dissolved in acetonitrile and measured immediately. The UV-1800 from Shimadzu with 1.0 cm quartz cuvettes (Hellma, suprasil) was used for the UV/vis measurements. ATR-FTIR spectra were recorded with a Jasco FT/IR-4700 spectrometer with a Jasco ATR Pro One unit containing a diamond crystal. Powder X-ray diffraction in transmission geometry was performed on a STOE STADIP diffractometer, in Debye−Scherrer geometry at room temperature. Samples were loaded in a 0.5 mm capillary. Diffraction patterns were measured with Cu Kα1 radiation (λ = 1.54060 Å) from a focusing Ge (111) monochromator and recorded with a position-sensitive Mythen 1K detector with 0.015° resolution in 2θ, operating at 40 kV and 40 mA. X-band EPR spectra of frozen solutions were recorded at 77 K using either a Bruker EMX X-band or a Bruker EMXnano X-band EPR spectrometer (sweep time of 60 s, microwave power of 1.0–2.5 mW, time constant of 1.28 ms, average microwave frequency of 9.635 GHz, modulation amplitude of 8 G). All samples were prepared in quartz capillary tubes and frozen in liquid nitrogen. Simulation of the EPR spectra were performed using EasySpin toolbox (5.2.13) for the Matlab program package.[49,50]

Ligands syntheses. Imidazolium chloride salts **1H.Cl** and **2H.Cl**, imidazolium hexafluorophosphate **3H.PF$_6$**, imidazolium tetrafluoroborate **4H.BF$_4$** and imidazolium

carboxylates **1-CO_2**, **2-CO_2**, **3-CO_2** and **4-CO_2** were synthesized following reported procedures.[17,24,36,51,52] The labelled imidazolium salt **^{13}C-1H.Cl** was prepared using the same procedure than for **1H.Cl** with 99% labelled ^{13}C- paraformaldehyde (Aldrich).[36]

Complexes syntheses. The synthesis of complexes (NHC)CuX_2 was accomplished using one of the following methods. Crystals were grown from slow diffusion of Et_2O into a solution of the complex in CH_2Cl_2.

Route a: Under nitrogen atmosphere, the imidazolium salt (0.20 mmol) was reacted with *t*BuOK (0.24 mmol) in dry THF (5 mL) for 30 min at room temperature. The solvent was removed in vacuo. The resulting free carbene was dissolved in dry toluene (10 mL) and stirred with a solution of CuX_2 (0.20 mmol) in dry DMF (1 mL), at room temperature for 16 h under nitrogen atmosphere. In vacuo, the reaction mixture was concentrated to 1 mL and Et_2O was added until a solid precipitated. The solid was collected by filtration and dissolved in CH_2Cl_2 (1 mL), filtered and precipitated again using Et_2O. After filtration, the solid was washed with Et_2O (2 x 2mL) and dried under vacuum.

Route a, one pot: Under nitrogen atmosphere, the imidazolium salt (0.20 mmol) was reacted with *t*BuOK (0.24 mmol) and $Cu(OAc)_2$ (0.20 mmol) in dry THF at room temperature. After 30 min, the reaction mixture was evaporated in vacuo and the solid was dissolved in CH_2Cl_2. The solution was filtered and pentane was added until a solid precipitated. The solid was collected by filtration, washed with Et_2O (2 x 2mL) and dried under vacuum.

Route b: To a solution of CuX_2 (0.10 mmol) in DMF (1 mL), solid imidazolium carboxylate (0.10 mmol) and toluene (5 mL) were added and the reaction mixture was stirred at room temperature for 16 h. Purification was identical to that described for route a.

(**1**)$Cu(OAc)_2$. Route a: Starting from imidazolium salt **1H.Cl** (138 mg, 0.32 mmol), *t*BuOK (44 mg, 0.39 mmol) and $Cu(OAc)_2$ (59 mg, 0.32 mmol) afforded the title complex as a royal blue powder (116 mg, 63%). Route a, one pot: Starting from imidazolium salt **1H.Cl** (92 mg, 0.22 mmol), *t*BuOK (30 mg, 0.27 mmol) and $Cu(OAc)_2$ (40 mg, 0.22 mmol) afforded the title complex as a royal blue powder (60 mg, 49%). Route b: Starting from imidazolium carboxylate **1-CO_2** (31 mg, 0.07 mmol) and $Cu(OAc)_2$ (13 mg, 0.07 mmol) yielded the title complex as a royal blue powder (18 mg, 44% yield). ^{1}H NMR (300 MHz, CD_2Cl_2): δ 10.7 (br), 8.6 (br), 8.3 (br), 7.6 (br), 7.4 (br), 2.6 (br), 1.3 (br) ppm. $^{13}C\{^1H\}$ NMR (75 MHz, CD_2Cl_2): δ 145.7, 140.9, 132.7, 130.6, 129.6, 127.6, 127.3, 125.3, 29.8, 24.9, 24.1 ppm. HR-MS: m/z calculated for

[(**1**)Cu(OAc)]$^+$ 510.2308; found 510.2308. Anal. Calcd for $C_{31}H_{42}CuN_2O_4$•1.2 H_2O: C, 62.91; H, 7.56; N, 4.73; O, 14.06. Found: C, 62.53; H, 8.34; N, 4.78; O, 14.03%.

(**^{13}C-1**)Cu(OAc)$_2$. Route a: Starting from imidazolium salt **^{13}C-1H.Cl** (95 mg, 0.22 mmol), *t*BuOK (30 mg, 0.27 mmol) and Cu(OAc)**$_2$** (40 mg, 0.22 mmol) afforded the title complex as a royal blue powder (72 mg, 57%). HR-MS: m/z calculated for [(**^{13}C-1**)Cu(MeCN)]$^+$ 493.2417; found 493.2487.

(**2**)Cu(OAc)$_2$. Route a: Starting from imidazolium salt **2H.Cl** (145 mg, 0.43 mmol), *t*BuOK (55 mg, 0.49 mmol) and Cu(OAc)**$_2$** (70 mg, 0.39 mmol) afforded the title complex as a royal blue powder (94 mg, 50%). Route b: Starting from imidazolium carboxylate **2-CO$_2$** (73 mg, 0.21 mmol) and Cu(OAc)$_2$ (38 mg, 0.21 mmol) yielded the title complex as a royal blue powder (75 mg, 74% yield). ^{1}H NMR (300 MHz, CD_2Cl_2): δ 10.8 (br), 7.7 (br), 7.4 (br), 7.11 (sh, s), 7.03 (sh, s), 6.92 (sh, s), 2.43 (sh, s), 2.36 (sh, s), 2.2 (br), 1.68 (sh, s) ppm. ^{13}C{^{1}H} NMR (75 MHz, CD_2Cl_2): δ 142.0, 140.0, 134.9, 131.4, 130.3, 129.6, 125.1, 123.2, 21.5, 21.4, 17.9, 17.3 ppm. HR-MS: m/z calculated for [(**2**)Cu(OAc)]$^+$ 426.1369; found 426.1377. Anal. Calcd for $C_{25}H_{30}CuN_2O_4$•0.3 H_2O: C, 61.10; H, 6.28; N, 5.70. Found: C, 60.89; H, 5.80; N, 5.61%.

(**3**)Cu(OAc)$_2$. Route b: Starting from imidazolium carboxylate **3-CO$_2$** (68 mg, 0.35 mmol) and Cu(OAc)$_2$ (62 mg, 0.34 mmol) yielded the title complex as a light blue powder (67 mg, 59% yield). ^{1}H NMR (300 MHz, CD_2Cl_2): δ 12.2 (br), 7.8 (br), 5.9 (br), 2.0 (br) ppm. ^{13}C{^{1}H} NMR (75 MHz, CD_2Cl_2): δ 141.3, 120.5, 23.9 ppm. HR-MS: m/z calculated for [(**3**)Cu(MeCN)]$^+$ 256.0875; found 256.0881. Anal. Calcd for $C_{13}H_{22}CuN_2O_4$•2.2 H_2O: C, 41.80; H, 7.12; N, 7.50. Found: C, 41.69; H, 5.99; N, 7.34%.

(**4**)Cu(OAc)$_2$. Route b: Starting from imidazolium carboxylate **4-CO$_2$** (68 mg, 0.35 mmol) and Cu(OAc)$_2$ (62 mg, 0.34 mmol) yielded the title complex as a light blue powder (161 mg, 93% yield). ^{1}H NMR (300 MHz, CD_2Cl_2): δ 7.8 (br), 5.0 (br), 2.33 (sh, s) ppm. ^{13}C{^{1}H} NMR (300 MHz, CD_2Cl_2): δ 129.4, 124.4, 38.8 ppm. HR-MS: m/z calculated for [(**4**)Cu(OAc)]$^+$ 218.0117; found 218.0115. Anal. Calcd for $C_9H_{14}CuN_2O_4$•0.9 H_2O: C, 36.77; H, 5.42; N, 9.53. Found: C, 36.92; H, 5.56; N, 9.05%.

(**1**)$CuCl_2$. Route a: Starting from imidazolium salt **1H.Cl** (109 mg, 0.26 mmol), *t*BuOK (31 mg, 0.39 mmol) and Cu(OAc)**$_2$** (35 mg, 0.26 mmol) afforded the title complex as an orange powder (62 mg, 46%). Route b: Starting from imidazolium carboxylate **1-CO$_2$** (57 mg, 0.13 mmol) and $CuCl_2$ (17 mg, 0.13 mmol) yielded the title complex as an orange powder (30 mg, 44% yield).

^{1}H NMR (300 MHz, CD_2Cl_2): δ 9.4 (br), 8.2 (br), 7.68 (t, 2H), 7.46 (d, 4H), 2.5 (br), 1.9 (br), 1.39 (d, J = 34.4 Hz, 24H) ppm. ^{13}C{^{1}H} NMR (75 MHz, CD_2Cl_2): δ 145.6, 138.6, 132.5, 130.5, 127.5, 125.3, 29.9, 26.1, 25.6 ppm. HR-MS: m/z calculated for [(**1**)Cu(MeCN)]$^{+}$ 492.2440; found 492.2428. Anal. Calcd for $C_{27}H_{36}Cl_2CuN_2$•0.25 $CuCl_2$: C, 58.26; H, 6.52; N, 5.03. Found: C, 58.44; H, 6.15; N, 5.28%.

(**1**)$CuBr_2$. Route a: Starting from imidazolium salt **1H.Cl** (78 mg, 0.18 mmol), *t*BuOK (27 mg, 0.22 mmol) and $CuBr_2$ (38 mg, 0.17 mmol) afforded the title complex as a dark yellow powder (75 mg, 71%). Route b: Starting from imidazolium carboxylate **1-CO$_2$** (56 mg, 0.13 mmol) and $CuBr_2$ (29 mg, 0.13 mmol) yielded the title complex as a pale green powder (28 mg, 35%).^{1}H NMR (300 MHz, CD_2Cl_2): δ 8.9 (br), 8.1 (br), 7.8 (br), 7.69 (m, 2H), 7.46 (dd, J = 11.8 Hz, 4H), 2.36 (dm, J = 33.9 Hz, 4H), 1.30 (dd, J = 22.6 Hz, 24H) ppm. ^{13}C{^{1}H} NMR (75 MHz, CD_2Cl_2): δ145.5, 138.1, 133.6, 133.1, 129.9, 128.6, 127.0, 126.1, 125.6, 30.0, 29.7, 25.2, 24.5, 23.7 ppm. HR-MS: m/z calculated for [(**1**)Cu(MeCN)]$^{+}$ 492.2440; found 492.2420. Anal. Calcd for $C_{27}H_{36}Br_2CuN_2$•0.28 $CuBr_2$: C, 48.08; H, 5.38; N, 4.15. Found: C, 48.31; H, 5.02; N, 4.22%.

[(**1**)$Cu(OH_2)_2$]$(NO_3)_2$. Route a: Starting from imidazolium salt **1H.Cl** (79 mg, 0.19 mmol), *t*BuOK (27 mg, 0.22 mmol) and $Cu(NO_3)_2$ (42 mg, 0.18 mmol) afforded the title complex as a pale turquoise powder (67 mg, 66%). Route b: Starting from imidazolium carboxylate **1-CO$_2$** (58 mg, 0.13 mmol) and $Cu(NO_3)_2$ (33 mg, 0.13 mmol) yielded the title complex as a pale turquoise powder (66 mg, 80%). Anal. Calcd for $C_{27}H_{40}CuN_4O_8$•2.6 H_2O: C, 52.05; H, 6.67; N, 8.99. Found: C, 52.06; H, 5.49; N, 8.95%.

(**1**)$Cu(BF_4)_2$. Route a: Starting from imidazolium salt **1H.Cl** (86 mg, 0.20 mmol), *t*BuOK (25 mg, 0.22 mmol) and $Cu(BF_4)_2$ (49 mg, 0.20 mmol) afforded the title complex as a pale blue powder (42 mg, 33%). Route b: Starting from imidazolium carboxylate **1-CO$_2$** (61 mg, 0.14 mmol) and $Cu(BF_4)_2$ (33 mg, 0.13 mmol) yielded the title complex as a pale turquoise powder (74 mg, 81%). Anal. Calcd for $C_{27}H_{36}B_2CuF_8N_2$: C, 51.83; H, 5.80; N, 4.48. Found: C, 51.94; H, 5.88; N, 4.31.

(**2**)$CuCl_2$. Route b: Starting from imidazolium carboxylate **2-CO$_2$** (78 mg, 0.22 mmol) and $CuCl_2$ (31 mg, 0.23 mmol) yielded the title complex as dark yellow powder (60 mg, 61% yield). ^{1}H NMR (300 MHz, CD_2Cl_2): δ 8.8 (br), 8.0 (br), 7.3 (br), 7.2 (br), 2.5 (br), 2.4 (br) ppm. ^{13}C{^{1}H} NMR (75 MHz, CD_2Cl_2): δ 143.2, 142.4, 140.0, 138.5, 135.1, 134.8, 130.8, 130.7, 130.1, 125.7, 21.6, 20.0, 19.9 ppm. HR-MS: m/z calculated for [(**2**)Cu(MeCN)]$^{+}$ 408.1501;

found 408.1484. Anal. Calcd for $C_{21}H_{24}Cl_2CuN_2 \cdot 0.15\ CuCl_2$: C, 54.95; H, 5.27; N, 6.10. Found: C, 54.66; H, 5.23; N, 6.09%.

Supporting Information: Powder XRD parameters, IR spectra, detailed ESI-MS spectra, details of simulated EPR spectra, NMR spectra and details of X-ray structural analysis for all reported structures.

Corresponding Author:

*E-mail for A.M.: martin.albrecht@dcb.unibe.ch

ORCID

Nathalie Ségaud: 0000-0002-9221-1416

Jonathan McMaster: 0000-0003-0917-7454

Gerard van Koten: 0000-0003-3293-8370 ??

Martin Albrecht: 0000-0001-7403-2329

Author Contributions

The manuscript was written through contributions of all authors. All authors have given approval to the final version of the manuscript.

Notes

The authors declare no competing financial interest.

Acknowledgements: We thank the European Research Council (CoG 615653), Marie Sklodowska-Curie Action for a fellowship to N.S. (grant 796762 "BiomCatOx"), and the University of Nottingham Propulsion Futures Beacon for funding towards this research.

References

(1) Arduengo, A. J.; Harlow, R. L.; Kline, M. A Stable Crystalline Carbene. *J. Am. Chem. Soc.* **1991**, *113*, 361–363.

(2) Arduengo, A. J.; Bertrand, G. Carbenes Introduction. *Chem. Rev.* **2009**, *109*, 3209–3210.

(3) Egbert, J. D.; Cazin, C. S. J.; Nolan, S. P. Copper N-Heterocyclic Carbene Complexes in Catalysis. *Catal. Sci. Technol.* **2013**, *3*, 912–926.

(4) Lazreg, F.; Nahra, F.; Cazin, C. S. J. Copper–NHC Complexes in Catalysis. *Coord. Chem. Rev.* **2015**, *293–294*, 48–79.

(5) Danopoulos, A. A.; Simler, T.; Braunstein, P. N-Heterocyclic Carbene Complexes of Copper, Nickel, and Cobalt. *Chem. Rev.* **2019**, *119*, 3730–3961.

(6) Jürgens, E.; Back, O.; Mayer, J. J.; Heinze, K.; Kunz, D. Synthesis of Copper(II) and Gold(III) Bis(NHC)-Pincer Complexes. *Zeitschrift für Naturforsch. B* **2016**, *71*, 1011.

(7) Arnold, P. L.; Rodden, M.; Davis, K. M.; Scarisbrick, A. C.; Blake, A. J.; Wilson, C. Asymmetric Lithium(I) and Copper(II) Alkoxy-N-Heterocyclic Carbene Complexes; Crystallographic Characterisation and Lewis Acid Catalysis. *Chem. Commun.* **2004**, *14*, 1612–1613.

(8) Hu, X.; Castro-Rodriguez, I.; Meyer, K. Copper Complexes of Nitrogen-Anchored Tripodal N-Heterocyclic Carbene Ligands. *J. Am. Chem. Soc.* **2003**, *125*, 12237–12245.

(9) Lake, B. R. M.; Willans, C. E. Remarkable Stability of Copper(II)−N-Heterocyclic Carbene Complexes Void of an Anionic Tether. *Organometallics* **2014**, *33*, 2027–2038.

(10) Kolychev, E. L.; Shuntikov, V. V; Khrustalev, V. N.; Bush, A. A.; Nechaev, M. S. Dual Reactivity of N-Heterocyclic Carbenes towards Copper(II) Salts. *Dalt. Trans.* **2011**, *40*, 3074–3076.

(11) Cheng, J.; Wang, L.; Wang, P.; Deng, L. High-Oxidation-State 3d Metal (Ti–Cu) Complexes with N-Heterocyclic Carbene Ligation. *Chem. Rev.* **2018**, *118*, 9930–9987.

(12) Yun, J.; Kim, D.; Yun, H. A New Alternative to Stryker's Reagent in Hydrosilylation: Synthesis, Structure, and Reactivity of a Well-Defined Carbene-Copper(II) Acetate Complex. *Chem. Commun.* **2005**, *41*, 5181–5183.

(13) Lin, S.-C. A.; Liu, Y.-H.; Peng, S.-M.; Liu, S.-T. Copper(II) Complexes of a Heterotopic N-Heterocyclic Carbene Ligand: Preparation and Catalytic Application. *J. Organomet. Chem.* **2018**, *859*, 52–57.

(14) Liu, B.; Xia, Q.; Chen, W. Direct Synthesis of Iron, Cobalt, Nickel, and Copper Complexes of N-Heterocyclic Carbenes by Using Commercially Available Metal Powders. *Angew. Chemie Int. Ed.* **2009**, *48*, 5513–5516.

(15) Smith, J. M.; Long, J. R. First-Row Transition Metal Complexes of the Strongly Donating

Pentadentate Ligand PY4Im. *Inorg. Chem.* **2010**, *49*, 11223–11230.

(16) O'Hearn, D. J.; Singer, R. D. Direct Synthesis of a Copper(II) N-Heterocyclic Carbene Complex in Air. *Organometallics* **2017**, *36*, 3175–3177.

(17) Voutchkova, A. M.; Feliz, M.; Clot, E.; Eisenstein, O.; Crabtree, R. H. Imidazolium Carboxylates as Versatile and Selective N-Heterocyclic Carbene Transfer Agents: Synthesis, Mechanism, and Applications. *J. Am. Chem. Soc.* **2007**, *129*, 12834–12846.

(18) Olguin, J.; Muller-Bunz, H.; Albrecht, M. Springloaded Porphyrin NHC Hybrid Rhodium(III) Complexes: Carbene Dissociation and Oxidation Catalysis. *Chem. Commun.* **2014**, *50*, 3488–3490.

(19) Wyer, E.; Gucciardo, G.; Leigh, V.; Müller-Bunz, H.; Albrecht, M. Comparison of Carbene and Imidazole Bonding to a Copper(I) Center. *J. Organomet. Chem.* **2011**, *696*, 2882–2885.

(20) Planchestainer, M.; Segaud, N.; Shanmugam, M.; McMaster, J.; Paradisi, F.; Albrecht, M. Carbene in Cupredoxin Protein Scaffolds: Replacement of a Histidine Ligand in the Active Site Substantially Alters Copper Redox Properties. *Angew. Chemie Int. Ed.* **2018**, *57*, 10677–10682.

(21) Tsuda, T.; Chujo, Y.; Takahashi, S.; Saegusa, T. Specific Two-Step Decarboxylation of Copper(I,II) β-Ketocarboxylates. A Novel Type of Regulation of the Decarboxylation of β-Keto Acids. *J. Org. Chem.* **1981**, *46*, 4980–4987.

(22) Cahiez, G.; Moyeux, A.; Gager, O.; Poizat, M. Copper-Catalyzed Decarboxylation of Aromatic Carboxylic Acids: En Route to Milder Reaction Conditions. *Adv. Synth. Catal.* **2013**, *355*, 790–796.

(23) Solvents that are not dry can be used for this synthesis, however a too high content of water has to be avoided as this will favor the formation of a green oil together with the blue solid.

(24) Naumann, S.; Schmidt, F. G.; Schowner, R.; Frey, W.; Buchmeiser, M. R. Polymerization of Methyl Methacrylate by Latent Pre-Catalysts Based on CO_2-Protected N-Heterocyclic Carbenes. *Polym. Chem.* **2013**, *4*, 2731–2740.

(25) Herrmann, W. A.; Köcher, C. N-Heterocyclic Carbenes. *Angew. Chemie Int. Ed. English* **2003**, *36*, 2162–2187.

(26) Hollóczki, O.; Terleczky, P.; Szieberth, D.; Mourgas, G.; Gudat, D.; Nyulászi, L. Hydrolysis of Imidazole-2-Ylidenes. *J. Am. Chem. Soc.* **2011**, *133*, 780–789.

(27) Alder, R. W.; Blake, M. E.; Chaker, L.; Harvey, J. N.; Paolini, F.; Schütz, J. When and How Do Diaminocarbenes Dimerize? *Angew. Chemie Int. Ed.* **2004**, *43*, 5896–5911.

(28) Schneider, H.; Schmidt, D.; Eichhöfer, A.; Radius, M.; Weigend, F.; Radius, U. Synthesis and Reactivity of NHC-Stabilized Iron(II)–Mesityl Complexes. *Eur. J. Inorg. Chem.* **2017**, *2017*, 2600–2616.

(29) Schaub, T.; Radius, U. Carbene Ligands and Complexes. In *Inorganic Syntheses*; John Wiley & Sons, Ltd, **2010**; pp 78–91.

(30) Kuehn, L.; Eichhorn, A. F.; Marder, T. B.; Radius, U. Copper(I) Complexes of N-Alkyl-Substituted N-Heterocyclic Carbenes. *J. Organomet. Chem.* **2019**, *881*, 25–33.

(31) Schaub, T.; Backes, M.; Radius, U. Nickel(0) Complexes of N-Alkyl-Substituted N-Heterocyclic Carbenes and Their Use in the Catalytic Carbon−Carbon Bond Activation of Biphenylene. *Organometallics* **2006**, *25*, 4196–4206.

(32) Karlin, K. D.; Hayes, J. C.; Juen, S.; Hutchinson, J. P.; Zubieta, J. Tetragonal vs. Trigonal Coordination in Copper(II) Complexes with Tripod Ligands: Structures and Properties of $[Cu(C_{21}H_{24}N_4)Cl]PF_6$ and $[Cu(C_{18}H_{18}N_4)Cl]PF_6$. *Inorg. Chem.* **1982**, *21*, 4106–4108.

(33) Solomon, E. I.; Heppner, D. E.; Johnston, E. M.; Ginsbach, J. W.; Cirera, J.; Qayyum, M.; Kieber-Emmons, M. T.; Kjaergaard, C. H.; Hadt, R. G.; Tian, L. Copper Active Sites in Biology. *Chem. Rev.* **2014**, *114*, 3659–3853.

(34) K. Nakamoto. *Infrared and Raman Spectra of Inorganic and Coordination Compounds*; Wiley: New York, **1986**.

(35) Sharrock, P.; Melník, M. Copper(II) Acetates: From Dimer to Monomer. *Can. J. Chem.* **1985**, *63*, 52–56.

(36) Hans, M.; Lorkowski, J.; Demonceau, A.; Delaude, L. Efficient Synthetic Protocols for the Preparation of Common N-Heterocyclic Carbene Precursors. *Beilstein J. Org. Chem.* **2015**, *11*, 2318–2325.

(37) Winter, A.; Thiel, K.; Zabel, A.; Klamroth, T.; Pöppl, A.; Kelling, A.; Schilde, U.; Taubert, A.; Strauch, P. Tetrahalidocuprates(II) – Structure and EPR Spectroscopy. Part 2: Tetrachloridocuprates(II). *New J. Chem.* **2014**, *38*, 1019–1030.

(38) Peisach, J.; Blumberg, W. E. Structural Implications Derived from the Analysis of Electron Paramagnetic Resonance Spectra of Natural and Artificial Copper Proteins. *Arch. Biochem. Biophys.* **1974**, *165*, 691–708.

(39) Mikuriya, M.; Nukada, R.; Morishita, H.; Handa, M. Chain Compounds Formed by the Reaction of Copper(II) Carboxylate $[Cu_2(O_2CR)_4]$ (R = $C(CH_3)_3$, CCl_3) and Bridging Ligand L (L = Pyrazine, 4,4′-Bipyridine, and 1,4-Diazabicyclo[2.2.2]Octane). *Chem. Lett.* **1995**, *24*, 617–618.

(40) Doedens, R. J. Structure and Metal-Metal Interactions in Copper(II) Carboxylate Complexes. *Prog. Inorg. Chem.* **1976**, 209–231.

(41) Youngme, S.; Cheansirisomboon, A.; Danvirutai, C.; Pakawatchai, C.; Chaichit, N. Polynuclear Paddle-Wheel Copper(II) Propionate with Di-2-Pyridylamine or 1,10-Phenanthroline: Preparation, Characterization and X-Ray Structure. *Inorg. Chem. Commun.* **2008**, *11*, 57–62.

(42) Fursova, E.; Romanenko, G.; Sagdeev, R.; Ovcharenko, V. Mononuclear Mn(II), Co(II), and Cu(II) Pivalates. *Polyhedron* **2014**, *81*, 27–31.

(43) Díez-González, S.; Stevens, E. D.; Scott, N. M.; Petersen, J. L.; Nolan, S. P. Synthesis and Characterization of $[Cu(NHC)_2]X$ Complexes: Catalytic and Mechanistic Studies of Hydrosilylation Reactions. *Chem. - A Eur. J.* **2008**, *14*, 158–168.

(44) Rao, V. M.; Sathyanarayana, D. N.; Manohar, H. X-Ray Crystal Structures of Some Adducts of Dimeric Copper(II) Acetate. Nature of the Copper–Copper Interaction. *J. Chem. Soc. Dalt. Trans.* **1983**, *10*, 2167–2173.

(45) Cheng, A. T. A.; Howald, R. A. Thermodynamics of Solvation of the Copper(II) Acetate Dimer. *Inorg. Chem.* **1975**, *14*, 546–549.

(46) Blue, E. D.; Gunnoe, T. B.; Petersen, J. L.; Boyle, P. D. Protonation of N-Heterocyclic Carbene Ligand Coordinated to Copper(I): Coordination Mode of Imidazolium Cation as a Function of Counterion as Determined by Solid-State Structures. *J. Organomet. Chem.* **2006**, *691*, 5988–5993.

(47) Su, H.-L.; Pérez, L. M.; Lee, S.-J.; Reibenspies, J. H.; Bazzi, H. S.; Bergbreiter, D. E. Studies of Ligand Exchange in N-Heterocyclic Carbene Silver(I) Complexes. *Organometallics* **2012**, *31*,

4063–4071.

(48) Lin, B.-L.; Kang, P.; Stack, T. D. P. Unexpected $C_{Carbene}$–X (X: I, Br, Cl) Reductive Elimination from N-Heterocyclic Carbene Copper Halide Complexes Under Oxidative Conditions. *Organometallics* **2010**, *29*, 3683–3685.

(49) Stoll, S.; Schweiger, A. EasySpin, a Comprehensive Software Package for Spectral Simulation and Analysis in EPR. *J. Magn. Reson.* **2006**, *178*, 42–55.

(50) Stoll, S.; Schweiger, A. ESR Spectroscopy in Membrane Biophysics. In *ESR Spectroscopy in Membrane Biophysics*; Hemminga, M. A., Berliner, L. J., Eds.; Springer: New York, **2007**; pp 299–322.

(51) Schaub, T.; Radius, U. Efficient C-F and C-C Activation by a Novel N-Heterocyclic Carbene–Nickel(0) Complex. *Chem. – A Eur. J.* **2005**, *11*, 5024–5030.

(52) Egashira, M.; Yamamoto, Y.; Fukutake, T.; Yoshimoto, N.; Morita, M. A Novel Method for Preparation of Imidazolium Tetrafluoroborate Ionic Liquids. *J. Fluor. Chem.* **2006**, *127*, 1261–1264.

Synopsis for Table of Contents Use Only

A new synthetic methodology for the preparation of Cu(II)-NHC complexes under aerobic conditions using imidazolium carboxylate precursors is reported. While spectroscopic analyses evidenced the formation of a Cu(II)–C_{NHC} bond, the complexes undergo specific structural rearrangement under recrystallization conditions.